Device Design and System Integration of a Two-Axis Water-immersible Micro Scanning Mirror (WIMSM) to Enable Dual-modal Optical and Acoustic Communication and Ranging for Underwater Vehicles

Xiaoyu Duan, Di Wang, Dezhen Song, and Jun Zou

***Abstract*— To address the communication and ranging challenges caused by underwater environment, we design dual modal devices for autonomous underwater vehicles (AUVs). The dual-modal design builds upon a co-axial ultrasonic and green laser beams which leverage different signal diverging patterns and different responses in the underwater environment by each modality to achieve robust adaptability. Here we report our recent progress in improving scanning and aiming capabilities for dual-modal beam steering. The core part is our Two-Axis Water-immersible Micro Scanning Mirror (WIMSM). We improve hinge design of WIMSM for larger scanning range. We incorporate high speed Hall effect sensor-based pose feedback channel to enable closed-loop scanning and aiming control. We design ultrasonic-assisted laser handshaking method to help AUVs to acquire optical underwater communication. We have prototyped our devices and tested them in a water tank. The initial results are promising.**

I. INTRODUCTION AND RELATED WORKS

Autonomous Underwater Vehicles (AUVs) have become popular due to many applications [1][2][3] such as oil & gas, environment protection, sea agriculture, defense, search & rescue, etc. However, underwater environment is very challenging for both communication and ranging, which significantly limits AUV's ability. AUV communication still relies on either slow acoustic channel or intermittent wireless communication after surfacing. Comparing to RF and optical/acoustic systems with diffused line of sight [4][5], co-axial and co-directional beams promise much better confidentiality. Also, acoustic ranging has low spatial resolutions. Although it is possible to leverage green-blue laser for both communication and ranging, laser signal requires precise aiming and scanning due to its narrow and collimated beam pattern. As a result, there is essentially no high-speed communication peer to peer line of sight mechanism between AUVs [6][7][8] when they are underwater.

We are interested in designing a dual-modal communication and ranging device for AUVs that combines both ultrasound and laser signals into a co-axial beam (Figures 1(a) and (b)). For communication, we can exploit the wide ultrasound beam to help aim the narrow laser beam at each other to achieve handshake, which is much faster than using ultrasound signals alone. For ranging, laser has high spatial resolution but may suffer when water is murky, where ultrasound signal can be a good backup.

To achieve the duo-modal design, a two-axis water-immersible micro scanning mirror (WIMSM) is a critical component that enables fast scanning and aiming operations of the co-axial dual-modal signal beams. In our previous work, we presented an initial design of two-axis WIMSMs, which consist of a reflective mirror plate mounted on a fixed-frame with four side torsion hinges and actuated by coils to enable fully water-immersible operation without any mechanical joints (Figure 1(c)). The design utilizes material resonance frequency to achieve efficient scanning. The prototype WIMSM has been used to demonstrate perform three main functions: optical transception, ultrasound transception, and dual beam co-steering [9].

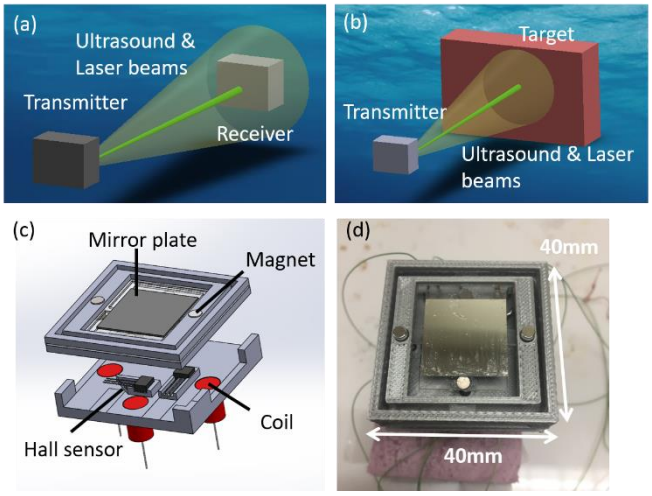

Figure 1. Illustration of the dual-modal scanning and aiming system for (a) communication and (b) ranging. (c) The sechmatic design and (d) photo of the previous WIMSM prototype [9].

However, the remaining key problem in the WIMSM development is to optimize its design for achieving precise control of scanning and aiming. Here, we report our recent progress in this direction. Firstly, a new optical and acoustic transceiver system suitable for underwater operation has been developed to serve as the testing platform for evaluating the beam steering performance of the WIMSM. Secondly, the WIMSIM has been re-designed with enhanced scanning

* The research is supported in part by National Science Foundation under NRI-1748161 and NRI-1925037.

X. Duan and J. Zou are with the Electrical and Computer Engineering Department, Texas A&M University, College Station, TX 77843, USA (e-mails: duanxiaoyu@tamu.edu, junzou@tamu.edu.

D. Wang and D. Song are with the Computer Science and Engineering Department, Texas A&M University, College Station, TX 77843, USA (e-mails: ivanwang@tamu.edu, dzsong@cs.tamu.edu).

performance and reduced package size. A new 3D scan pose sensor is employed to enable the proportional–integral–derivative (PID) control of the angular pose the WIMSM with higher accuracy. Lastly, capitalizing upon the complementary nature of the ultrasound and laser beam patterns, an initial demonstration of automatic searching, aiming and communication has been successfully achieved in experiments. The results demonstrated that the two-axis WIMSM can perform scanning and aiming with desirable accuracy, which will be useful for the development of dual-modal communication and ranging devices for AUVs.

II. System Design

As shown in Figure 2(a), the frontend of the optical and ultrasound transceiver system consists of an optical transceiver, an ultrasound transceiver and a WIMSM. The optical transceiver includes a laser diode as the light source, a photodiode as the detector and an optical beam splitter (OBS) to combine the forward and returning paths of the laser signal. To generate co-axial laser/ultrasound beam, the ultrasound transceiver consists of a piezoelectric ring transducer located in front of the OBS. The laser/ultrasound beams are reflected and steered by the WIMSM around two orthogonal axes. A 3D integrated scan pose sensor is used to monitor the two rotation angles of the reflecting mirror plate. Figure 2(b) shows an assembled prototype of the frontend.

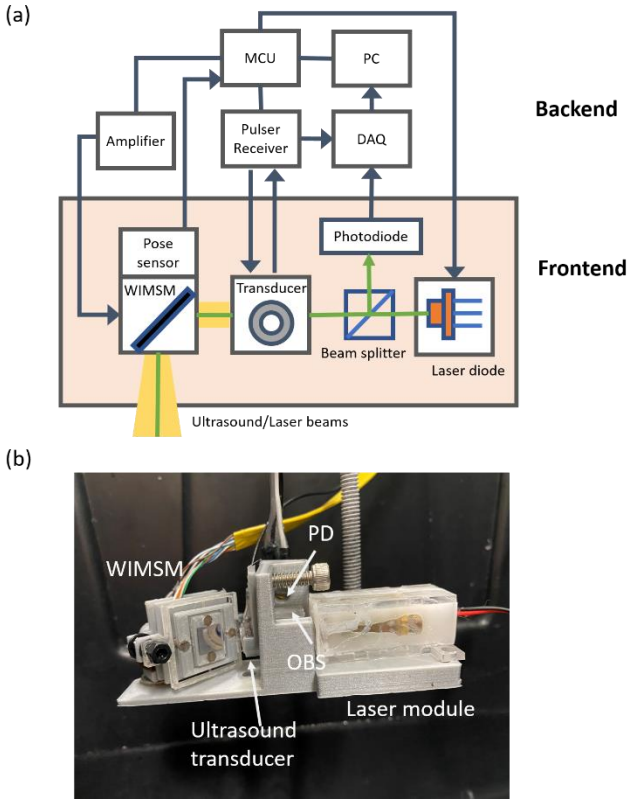

Figure 2. (a) Block diagram of the WIMSM-based optical and ultrasound transceiver. (b) A new prototype of the frontend of the optical and acoustic transceiver system.

In the backend, the ultrasound pulser-receiver is triggered by the microcontroller unit (MCU) to drive the ring transducer. Ultrasound signals received by the transducer are amplified by the pulse-receiver. The laser diode can operate in both CW (continuous wave) and pulsed mode, which is controlled by the MCU. The received ultrasound (from the transducer) and laser signals (from the photodiode) are sampled by the data acquisition card (DAQ) housed in the PC. The MCU drives the WIMSM through its digital-to-analog converter (DAC) port and takes readings from the 3D scan pose sensor to provide close-loop control for the WIMSM. The PC and MCU communicates with each other through their ethernet ports.

For ranging operations, a two-axis scanning operation of a single WIMSM unit is sufficient. However, underwater communication requires a pair of transceivers to search and lock to each other. Therefore, we have developed software to enable dual modal automatic searching, aiming and communication between two frontend modules (Figure 8). The two frontend modules are configured as the transmitter and receiver, respectively. Their operations are controlled and synchronized by the back module. The key design here is to utilize ultrasound's wide beam pattern to assist laser beam to pinpoint the receiver's relative poses needed for optical communication. First, the transmitter needs to search for the receiver. The WIMSM in the transmitter emits and scans the ultrasound/laser beams within its full working range. The ultrasound signals detected by the receiver at each scan pose are used to map out the ultrasound peak, which provides a rough estimation of the receiver's location. Next, the WIMSM in the transmitter is programmed to fine scan the laser beam within a smaller region surrounding the ultrasound peak location. The laser beam is suitable for fine-range localization due to its small beam divergence. Lastly, the steering and aiming of the laser beam is accomplished with the PID control. Depending on the actual working conditions, several iterations of fine-range searching and aiming may be needed to achieve a successful handshake between the two frontend modules.

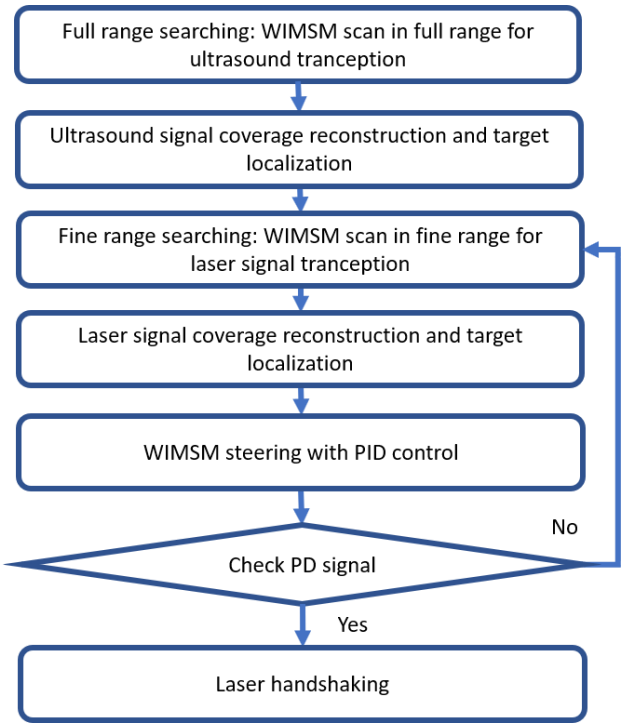

Figure 3. Flow chart of the dual modal searching, aiming and handshaking process between two frontend modules.

III. WIMSM Development

A. Design, fabrication and testing

Figure 4 show the pictures of the top and side views of the new WIMSM. The mirror plate is connected to an inner frame with a pair of flexible polymeric hinges. The inner frame is supported on an outer frame by a second pair of flexible polymeric hinges. This configuration offers the mirror plate with two-DoF (degree of freedom) rotation around two orthogonal scanning axes (X and Y). The rotation of the mirror plate around the X and Y axes is designated as Tilt and Pan, respectively. The mirror plate is driven by 2 pairs of electromagnetic actuators that consist of permanent magnets and inductor coils. Two improvements have been made in the redesigned WIMSM. Firstly, the dimensions of the polymer hinges are optimized to provide a wider scanning range and a more balanced static and dynamic scanning performance, thereby enlarging the range of coverage by beam steering. Secondly, the two 1D scan pose sensors have been replaced by a single 3D sensor with a wider linear range to accommodate the enlarged scanning range. This also makes it possible to reduce the mirror package size from 40×40×20 mm^3 [9] down to 25×25×20 mm^3.

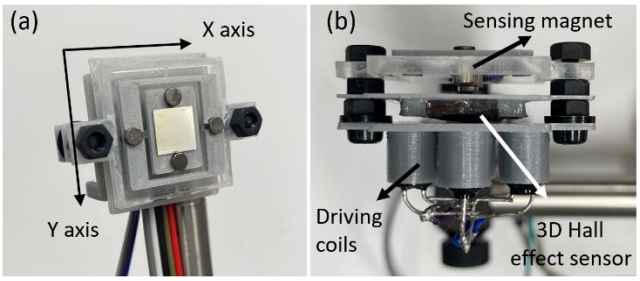

Figure 4. (a) Front view and (b) side view of the new WIMSM.

The characterization of the WIMSM is performed using a laser-tracing method [9][10]. The rotation angle of the mirror plate is calculated from the deviation of the laser trace reflected on the reading screen. The resonance frequencies of both axes are characterized by applying an AC driving current with a constant amplitude and a sweeping frequency from DC up to 45 Hz. The resonance frequency is defined as the driving frequency when the rotation angle reaches its maximum. As listed in Table I, the resonance frequency of the two axes are determined to be 32 Hz and 9 Hz, respectively. Driven by a 170-mA current at their resonance frequencies, the optical rotation angle in Pan and Tilt reaches ±16.5° and ±8.0°, respectively, which are much larger than ±8.5° and ±6.5° obtained before [9].

TABLE I. Resonance Frequencis and Scanning Angles

	Resonance frequency	***Maximal scanning angle***
Pan	9 Hz	±16.5° (AC 170 mA)
Tilt	32 Hz	±8.0° (AC 170 mA)

With both axes actuated at their resonace frequencies, the laser scanning pattern of the WIMSM is characterized. The waveform of the two driving currents and the resulting scanning pattern are shown in Figure 5. It is clear that the laser scanning pattern has some distortions, which are caused by small imbalance in the electromagnetic force between the driving magnets. Nonetheless, the laser scanning pattern is stable and repeatable. Therefore, this distortion should not be a big concern, which can be monitored by the scan pose sensor and compensated during data processing.

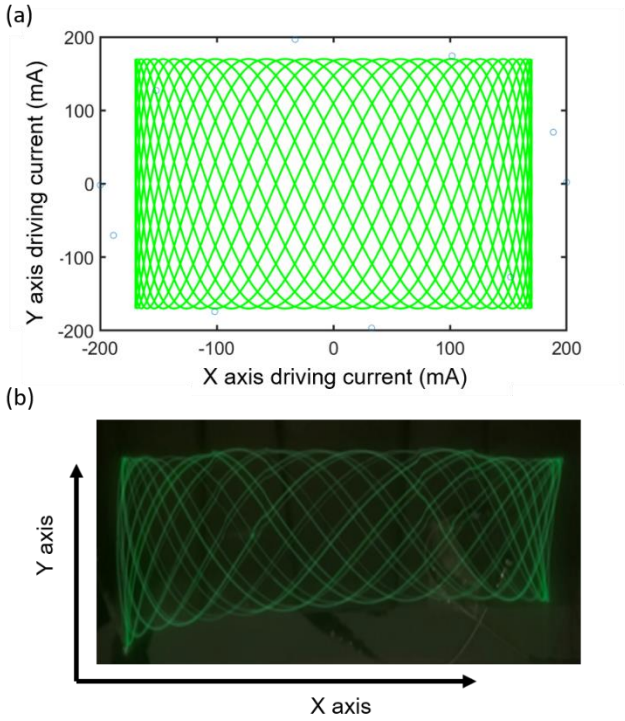

Figure 5. (a) The driving signals and (b) the scanning pattern of WIMSM under water.

B. Pose feedback

Ideally, the scan pose sensor should provide direct pose readings of the mirror plate or steered beams. However, the viable choice is to employ a 3D Hall-effect sensor to detect the magnetic field strength (in three dimensions) of the sensing magnet attached onto the back of the mirror plate, which allows us to infer the pose of the WIMSM in a contactless way (Figure 6(a)). To characterize the sensitivity, linearity and repeatability of the scan position sensor, both axes of the WIMSM are driven at their resonance frequencies. The pose of the mirror plate is monitored in real time with the laser-tracing method. The laser beam reflected by the mirror plate is directed to a checkerboard. The laser trace on the checkerboard is continuously recorded by a camera, from which the optical rotation angles in Pan and Tilt are calculated. Figure 6 (b) and (c) show the two magnetic field readings (B_x and B_y) vs. the mirror plate pose, respectively. It can be clearly seen that they closely track the change of the mirror plate pose. B_x increases almost linearly with the rotation angle in Pan and is not significantly affected by the rotation angle in Tilt. In contrast, B_y increases almost linearly with the rotation angle in Tilt and is not significantly affected by the rotation angle in Pan. From Figure 6(c), the rotation in Tilt is somewhat less stable than in Pan, because the Tilt rotation occurs in the inner frame and is slightly affected by the Pan rotation in the outer frame. Nevertheless, the scan pose sensor readings have good

linearity and repeatability, which are useful for monitoring the pose of the mirror plate for the implementation of the closed-loop control.

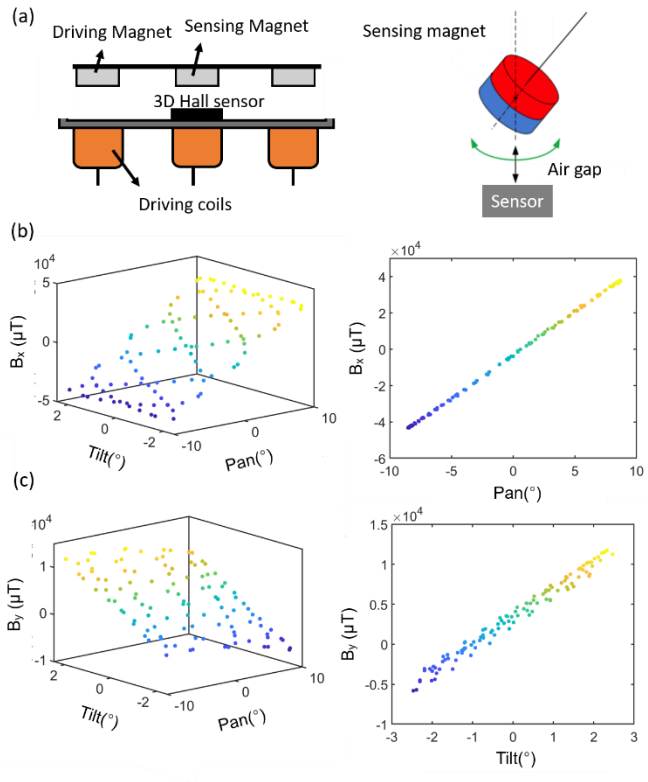

Figure 6. (a) Schematic diagram of the scan pose sensor. (b) Pose sensor reading (B_x) at different Pan and Tilt angles. (c) Pose sensor reading (B_y) at different Pan and Tilt angles.

C. *PID control*

To precisely adjust the direction of optical-acoustic beam steering, a PID controller implemented in C^{++} on MCU is used to control the two axes of WIMSM. Because the two axes of the WIMSM are mechanically decoupled and independently actuated, each of them can be controlled by a single-input and single-output PID controller. The controllers' inputs are the pose sensor readings (B_x and B_y) determined by the peak location of amplitude peak in the laser signal map. The process variables are the sensed pose outputs and the control variables are the driving voltage of WIMSM. A typical step response of the two axes of WIMSM is shown in Figure 7. B_x varies from -14232μT to -9563μT, representing a pan rotation from -2.3° to -1.1°. Whereas B_y drops from 7945μT to 112μT, indicating that the tilt angle changes from +0.9° to -1.1°. The response time of the 2-axis rotation in the system is around 2 s, which should be adequate for laser aiming when the receiver module remains static at a fixer position.

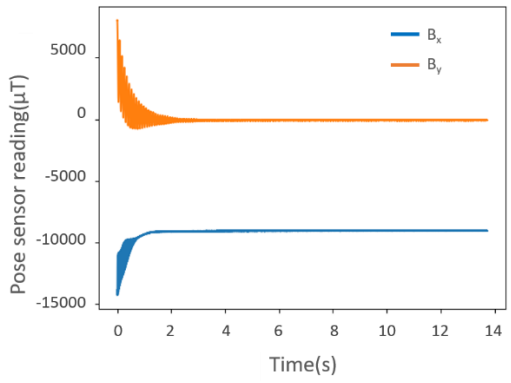

Figure 7. The response of the scan pose sensor during PID control of the WIMSM.

IV. EXPERIMENTS

A. *Testing setup*

Figure 8(a) and (b) show the schematic diagram and the top view of the testing setup for characterizing the co-axial ultrasound and laser beam steering by the WIMSM. Two frontend modules serve as transmitter and receiver respectively, which are controlled by one backend module. The transmitter sends co-axial ultrasound and laser beams, while the receiver waits for the signals. The WIMSM in the transmitter is driven by the MCU and controlled by the PID controller. The ultrasound transducer is actuated with a pulser/receiver for signal transception. The laser diode is driven by the MCU for both CW and pulsed operation. The received ultrasound and laser signals are digitized by the DAQ card. The pulser/receiver is configured into the pulse-echo mode and synchronized with the scan pose sensor.

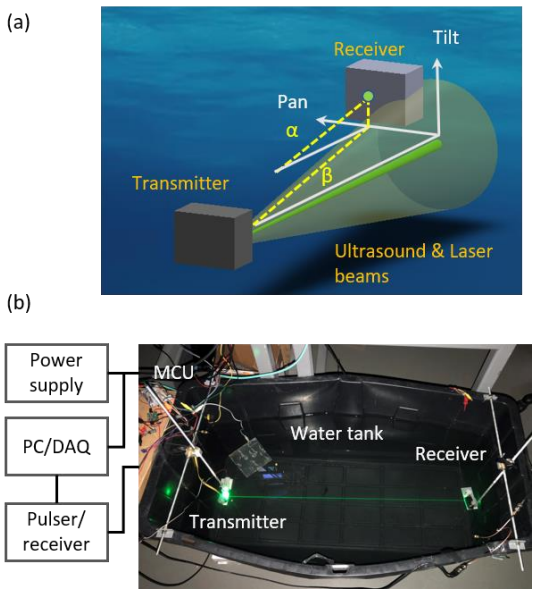

Figure 8. (a) Schematic diagram and (b) top view of the testing setup to characterize the ultrasound and laser beam steering by the WIMSM

B. *ultrasound and laser beam steering coverage test*

The test begins with a full range scan of the WIMSM, which covers ±16.5° in Pan and ±8.0° in Tilt. At each scan point, the receiver acquires the ultrasound signal from the transmitter. The peaks of the ultrasound signals are used to reconstruct the ultrasound amplitude image. Due to the low density of scanning pattern, a surface fitting is applied to localize the center of ultrasound peak in the coverage (Figure 9(a)). In this test, the resulting center location of the received ultrasound signal is -10.8° in Pan and -2.9° in Tilt. The laser signal center location (Figure 9(b)) appears nearby at -11.5° in Pan and -3.0° in Tilt. The deviation between the centers of ultrasound and laser signals is mainly caused by the

misalignment of the two beams after being reflected by the WIMSM. Meanwhile, the time delay among the ultrasound transducer and photodiode and other components may result in additional mismatch in the localization of the two beams. Nevertheless, the ultrasound coverage can still provide a good guidance for steering and aiming the laser beam towards the receiver module. To pinpoint the exact location of the receiver module, a fine-range scanning around the ultrasound peak location (±3.0° in Pan and ±2.5° in Tilt) is conducted. Figure 9 shows the reconstructed ultrasound and laser peak amplitude maps. While the peak of the ultrasound signals is hard to identify, the laser signal provides a much more pronounced peak due to the narrow beam.

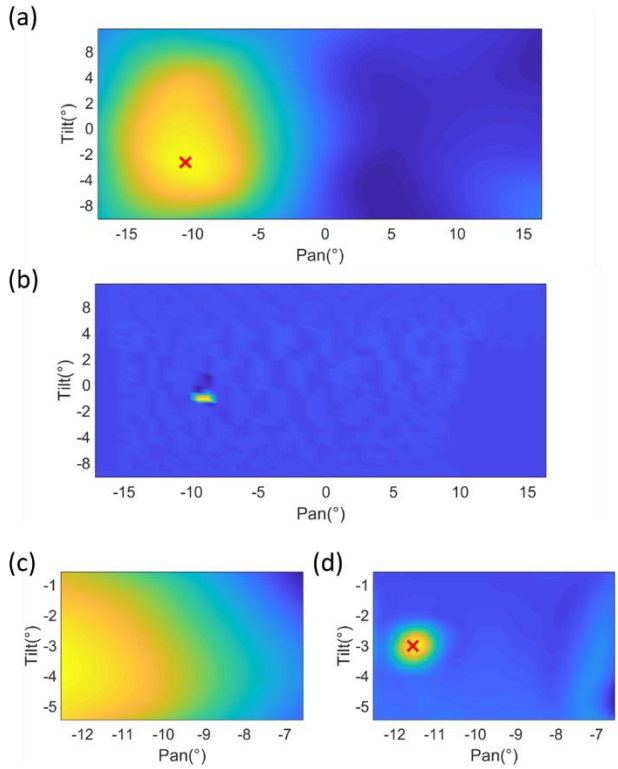

Figure 9. Reconstructed signal peak distribution map of (a) full-range ultrasound scan, (b) full-range laser scan, (c) fine-range ultrasound scan, and (d) fine-range laser scan. The red "x" signs represent the center of signal peak.

C. Searching, aiming and communication test

An initial experiment of automatic searching, aiming and handshaking has been conducted. The two frontend modules are configured as the transmitter and receiver (Figure 10), respectively. A red LED (light emitting diode) is used as an indicator of successful handshaking. It will light up when the laser emitting from the transmitter is delivered onto the photodetector inside the receiver. First, both the transmitter and receiver are placed face to face on each side of the water tank, respectively. The receiver is located at random location with respect to the transmitter (Figure 10(a)). The transmitter sends and scans co-axial ultrasound (not visible) and laser (green) beams within the full scanning range of the WIMSM (e.g., ±16.5° in Pan and ±8° in Tilt) (Figure 10(b)). The amplitude of the ultrasound signals detected by the receiver at different scanning poses of the WIMSM is used to reconstruct an ultrasound mapped image (see Figure 9(a)). The location of the peak ultrasound amplitude is determined, which serves as an initial estimation of the location of the receiver. Next, the laser beam (together with the ultrasound beam) is steered toward the direction of the ultrasound peak (Figure 10(c)) and one or multiple fine laser scans of the surrounding region (±3.0° in Pan and ±2.5° in Tilt) are conducted (Figure 10(d)). The amplitude of the laser signals detected by the receiver at different scanning poses of the WIMSM is used to reconstruct a laser mapped image (see Figure 9(b)). The location of the peak laser amplitude is used to pinpoint the location of the receiver. Finally, with the PID feedback control, the laser beam is steered towards the receiver. Once the laser is detected by the photodetector, the aiming and handshaking between the transmitter to the receiver module are accomplished, which is indicated by the lighting-up of the red LED indicator. For verification, after one cycle of searching, aiming and handshaking is completed, the receiver is moved to another (random) location and the above process is successfully replicated (Figure 10 (f)).

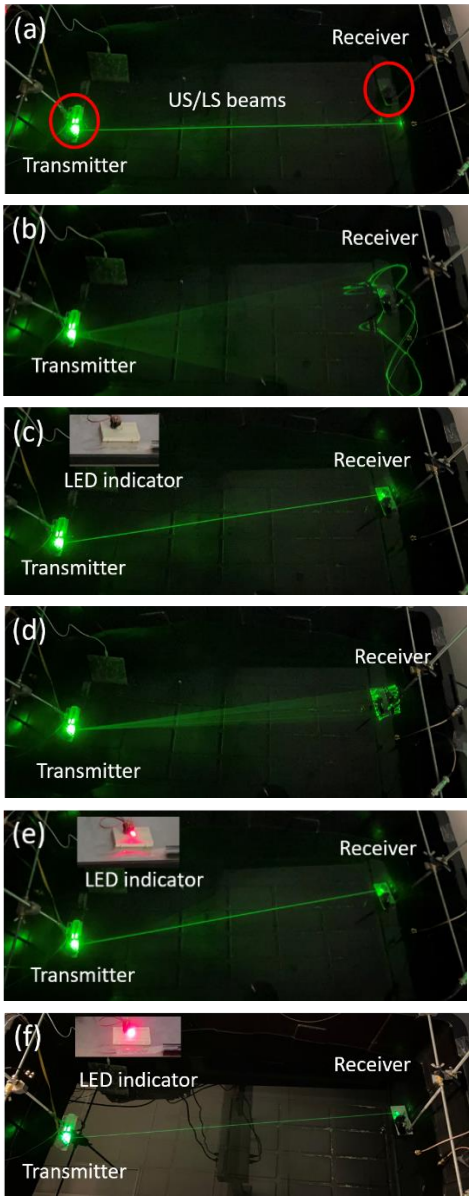

Figure 10. Photos showing the major operation steps of the searching, aiming and handshaking experiment: (a) Start pose. (b) Full-range searching. (c)

Steering after full range searching. (d) Fine-range searching. (e) Steering and handshaking with laser signals. (f) Successful handshaking at a different receiver location.

V. Conclusion and Future works

In summary, we presented the device design and system integration of a WIMSM for dual-modal optical and acoustic communication for underwater vehicles. The system was built upon the co-axial ultrasound and laser beam steering enabled by the new two-axis WIMSM. We optimized the mirror design with a smaller package and improved jointless hinge design. We integrated a 3D Hall-effect sensor to enable scanning and aiming control to provide controllable coverage in both ranging and communication applications. We designed ultrasonic-assisted laser handshaking to enable AUVs to obtain optical communication capability. We prototyped the system and tested it in a water tank. The experimental results demonstrated promising results.

In the future, we will further develop WIMSM to improve scanning range, speed, and accuracy and reduce size. We will integrate our WIMSM device to a testing AUV and develop a more advanced signal acquisition and handshaking algorithm by utilizing the additional 3 DoFs brought by the AUV. We will develop medium access control protocol and high-level protocols to make it compatible with existing network protocol stacks. We will also develop dual modal ranging verification algorithm to ensure that we can leverage the benefit of both modalities when mapping underwater environments.

Acknowledgment

We would like to thank Yue Ou for his help in experiments and prototype construction.

References

[1] F. S. Hover et al., “Advanced perception, navigation and planning for autonomous in-water ship hull inspection,” Int. J. Rob. Res., vol. 31, no. 12, pp. 1445–1464, 2012.

[2] H. Johannsson, M. Kaess, B. Englot, F. Hover, and J. Leonard, “Imaging sonar-aided navigation for autonomous underwater harbor surveillance,” in 2010 IEEE/RSJ International Conference on Intelligent Robots and Systems, 2010.

[3] H. Horimoto, T. Maki, K. Kofuji and T. Ishihara, "Autonomous Sea Turtle Detection Using Multi-beam Imaging Sonar: Toward Autonomous Tracking," 2018 IEEE/OES Autonomous Underwater Vehicle Workshop (AUV), Porto, Portugal, pp. 1-4, 2018.

[4] Z. Zeng, S. Fu, H. Zhang, Y. Dong and J. Cheng, "A Survey of Underwater Optical Wireless Communications," in IEEE Communications Surveys & Tutorials, vol. 19, no. 1, pp. 204-238, Firstquarter 2017.

[5] N. Farr, A. Bowen, J. Ware, C. Pontbriand and M. Tivey, "An integrated, underwater optical /acoustic communications system," OCEANS'10 IEEE SYDNEY, Sydney, NSW, Australia, 2010.

[6] L. Wallace, A. Lucieer, C. Watson, and D. Turner, “Development of a UAV-LiDAR System with Application to Forest Inventory,” Remote Sensing, vol. 4, no. 12, pp. 1519–1543, 2012.

[7] M. V. Jakuba et al., “Long-baseline acoustic navigation for under-ice autonomous underwater vehicle operations,” Journal of Field Robotics, vol. 25, no. 11–12, pp. 861–879, 2008.

[8] N. R. Rypkema, E. M. Fischel and H. Schmidt, "Closed-Loop Single-Beacon Passive Acoustic Navigation for Low-Cost Autonomous Underwater Vehicles," 2018 IEEE/RSJ International Conference on Intelligent Robots and Systems (IROS), pp. 641-648, Madrid, 2018.

[9] X. Duan, D. Song and J. Zou, "Steering Co-centered and Co-directional Optical and Acoustic Beams with a Water-immersible MEMS Scanning Mirror for Underwater Ranging and Communication*," 2019 International Conference on Robotics and Automation (ICRA), Montreal, QC, Canada, pp. 6582-6587, 2019

[10] C.-H. Huang, J. Yao, L. V. Wang, and J. Zou, “A water-immersible 2-axis scanning mirror microsystem for ultrasound and photoacoustic microscopic imaging applications,” Microsyst. Technol., vol. 19, no. 4, pp. 577–582, 2012.

[11] S. Xu, C.-H. Huang, and J. Zou, “Microfabricated water-immersible scanning mirror with a small form factor for handheld ultrasound and photoacoustic microscopy,” J. Micro/Nanolithogr. MEMS MOEMS, vol. 14, no. 3, p. 035004, 2015.